Development of a Process Window for Minimizing Volatile-Induced Surface Porosity in the Resin Transfer Molding of a Benzoxazine/Epoxy Blend

M. Anders*, J. Lo, T. Centea, and S.R. Nutt

M.C. Gill Composites Center, Viterbi School of Engineering, University of Southern California, 3651 Watt Way, VHE-708, Los Angeles, California, 90089, United States.

*Corresponding author's e-mail: anders@usc.edu

Abstract:

We consider the design of cure temperature cycles for the resin transfer molding (RTM) of carbon-fiber laminates using a prototype blended resin that requires a two-stage cure cycle to prevent volatile-induced surface porosity. While a two-stage cure cycle improves surface quality, it also adds significant cycle time to the processing, therefore a methodology to identify the fastest cure cycle that avoids surface porosity is desired. We propose the development of a process map, which enables the design of cure cycles with optimal intermediate dwells. First, the resin cure kinetics are characterized using a "model-free" isoconversional method. Next, thermogravimetric analysis (TGA) and rheological dynamic analysis (RDA) are used to determine a threshold mechanical state, above which the release of volatile species can no longer occur. Finally, molded composite samples are fabricated in a highly-instrumented lab-scale RTM tool, which features temperature and pressure sensors, as well as a transparent mold wall that enables *in situ* observation of surface porosity formation. The results are combined into a process map that shows, for any intermediate dwell temperature, the allowed dwell time window to produce porosity-free parts. Furthermore, by considering an RTM tool with a given tolerance for temperature control, the process window can be used to design the fastest cure cycle that properly accommodates for the magnitude of thermal gradients present. Finally, to validate the effectiveness of this approach, a molded sample is

Please cite this article as: M. Anders, J. Lo, T. Centea, and S.R. Nutt, **"Development of a Process Window for Minimizing Volatile-Induced Surface Porosity in the Resin Transfer Molding of a Benzoxazine/Epoxy Blend",** Journal of Advanced Materials vol. 1 (2016) ISSN 1070-9789

fabricated using an "optimized" cure cycle designed with the process map and the surface quality is compared to the baseline cases. Altogether, the work clarifies the complex mechanisms that can lead to surface porosity formation during the RTM processing of a novel resin, and provides a practical, science-based methodology for identifying process modifications that can reduce defect levels.

1. INTRODUCTION

Resin transfer molding (RTM) is a popular composite manufacturing technique for producing small to medium sized parts with low microstructural defect levels, excellent surface finishes, and potentially complex geometries [1]. Voids are the most common type of defect encountered in RTM, and are often a result of incomplete preform saturation during injection. Air can become trapped within the mold cavity due to improper injection pressure [2] or gate/vent placement [3], and considerable efforts have been made to develop models and protocols that ensure successful injection for arbitrary mold geometries. However, voids can also arise from another source, namely volatiles released by the resin after injection, during the curing phase of the RTM process.

In the present study, we investigate volatile-induced porosity in context of a prototype resin, currently under development for RTM of primary aerospace structures. This blended formulation contains both benzoxazine and epoxy constituents, as well as a proprietary catalyst. The benzoxazine component imparts excellent resistance to moisture uptake and chemically aggressive environments, as well as favorable flammability, smoke, and toxicity (FST) properties. The resin's epoxy component acts to toughen the otherwise brittle benzoxazine matrix, and also increases the T_g by raising the maximum theoretical cross-link density [4]. While this resin has many potential benefits compared to standard aerospace epoxies, it also presents some additional challenges. One concern is an increased resin volatility, which must be suppressed by the positive hydrostatic pressure applied

during RTM processing. A previous study [5] has shown that the minimum "critical pressure" required to suppress volatile release for this resin is ~200 kPa (absolute).

While the minimum required pressure is easily within the limits of most standard RTM systems, the challenge lies in maintaining mold cavity pressure during chemical cure shrinkage caused by polymerization. Despite the total cure shrinkage of this resin being relatively low (around 1% [6]) compared to other thermoset resins, the density increase is sufficient to create a loss of cavity pressure during cure.

Previous work by the authors [5] described how the combined effects of increased resin volatility and shrinkage-induced pressure drops led to volatile-induced surface porosity. The severity of this type of defect is determined by the timing of the inevitable pressure drop relative to the gelation of the resin. In the presence of thermal gradients (which exist to varying extents in almost all molding tools), the progression of cure in the coldest regions of the mold cavity lags behind that of the hotter regions. When the thermal gradient is in the through-thickness direction (as is the case for the molding tool used in this study), the cold side of the part is susceptible to surface porosity formation because the viscosity at that location can still be low (facilitating void nucleation and growth) when the cumulative shrinkage of the entire part becomes enough to cause a pressure drop.

During RTM processing, if the mold is ramped directly to the high-temperature dwell (185°C) after resin injection (at 110°C), even modest thermal gradients (5-10°C) cause the cure gradient to become large enough that the cold side is still at low viscosity when the pressure drop occurs, resulting in volatile release at that surface. The previous study also showed that, conversely, if a 3 hour intermediate dwell at 130°C is included in the cure cycle, surface porosity is almost entirely avoided. The intermediate dwell acts to progress the cure reaction at a reduced rate, limiting the amount by which the cold side lags when the pressure drop finally occurs. By raising the viscosity

above a threshold value, the tendency for volatile release greatly diminishes and the formation of voids is inhibited.

This modified cure cycle, while effective at suppressing surface porosity, has the drawback of an almost tripled cycle time compared to the baseline cure cycle. From a manufacturing standpoint, this translates to reduced output and increased costs. Therefore, a methodology to minimize both surface porosity and cycle time is desired. The goals of this study are first, to describe the criteria that suppress the formation of surface porosity, and second, to develop a process map, which enables the design of cure cycles that prevent surface porosity using the minimum cycle time, given the magnitude of thermal gradients present in the tool.

The first step of our approach was to model the kinetics of the resin curing reaction to enable prediction of the reaction rate for arbitrary temperature cycles. A purely empirical "model-free" isoconversional method was applied, using differential scanning calorimetry (DSC) scans of the cure exotherm. Next, the cure kinetics model was applied to rheological dynamic analysis (RDA) and thermogravimetric analysis (TGA) data, to determine the degree of cure values corresponding to gelation and to the cessation of volatile release. Then, molded samples were fabricated with extended dwells at a range of intermediate temperatures, to determine the maximum dwell time before a pressure drop occurs. A lab-scale RTM tool was used, which includes temperature and pressure sensors, as well as a glass tool-plate on one side that enables direct visual observation of surface porosity formation and other in-mold phenomena. Finally, the results were combined into a process map, an "optimized" cycle was designed, and a molded sample was fabricated with the new cure cycle to validate the utility of the process map. The results show that this methodology can be used to successfully develop faster cure cycles, with negligible reduction in surface quality.

Please cite this article as: M. Anders, J. Lo, T. Centea, and S.R. Nutt, **"Development of a Process Window for Minimizing Volatile-Induced Surface Porosity in the Resin Transfer Molding of a Benzoxazine/Epoxy Blend",** Journal of Advanced Materials vol. 1 (2016) ISSN 1070-9789

2. EXPERIMENTAL METHODS

2.1. Thermal Characterization

The heat of reaction was measured via DSC (Q2000, TA Instruments) using 5 – 10 mg samples of resin in hermetically sealed aluminum pans. Temperature cycles consisted of linear ramps from 35 to 315°C at rates of 5, 7, and 10°C/min. Rates above those normally seen in RTM processing were used for the purpose of maximizing signal quality. TGA (Q5000IR, TA Instruments) tests were performed at ambient pressure on samples weighing 40 ± 0.5 mg to determine the mass loss due to volatilization. Temperature cycles consisted of linear ramps from 35 to 315°C at rates of 1, 2, and 3°C/min. The viscosity was measured using a rheometer (AR2000ex, TA Instruments) with disposable aluminum parallel plate fixtures and the same temperature cycles as the TGA tests. All data processing and cure modeling was performed in MATLAB (R2014b, The Mathworks, Inc.).

2.2. RTM Manufacturing Trials

Molded composite samples were fabricated under a variety of cure temperature cycles. All cure cycles started at 110°C, used 2°C/min ramps, and ended with a 60 minute dwell at 185°C. The cycles differed in the time and temperature of an intermediate dwell, summarized in Table 1. Cycle A is considered the baseline case, with no intermediate dwell, and is included to demonstrate the need for a 2-stage cycle and to show how surface porosity forms when rapid gelation is induced. Cycle B corresponds to previous work [5], and represents the cure cycle that has been shown to minimize surface porosity. Cycles C through G, with "extended" dwells, denote intermediate dwells that were held until the pressure drop occurred, and were used to determine the maximum possible hold time at each intermediate temperature as described in section 6. Finally, cycle H was designed using the

methods described in this paper, and represents an attempt at reducing the cycle time compared to cycle B while achieving similarly low surface porosity levels.

Table 1: List of tested cure cycles.

Cure cycle	Intermediate dwell temperature	Intermediate dwell time
A	None	None
B	130°C	180 minutes
C	130°C	Extended
D	140°C	Extended
E	150°C	Extended
F	160°C	Extended
G	170°C	Extended
H	150°C	45 minutes

The lab-scale RTM used for fabricating molded samples is shown in Figure 1. The main tool body is an aluminum block containing heating elements, inlet/outlet ports, thermocouples, and a pressure sensor. A "picture frame" style spacer plate determines the thickness (3.2 mm) and in-plane dimensions (76 × 127 mm) of the molded part, and a 20 mm thick tempered glass plate acts as the second tool-face.

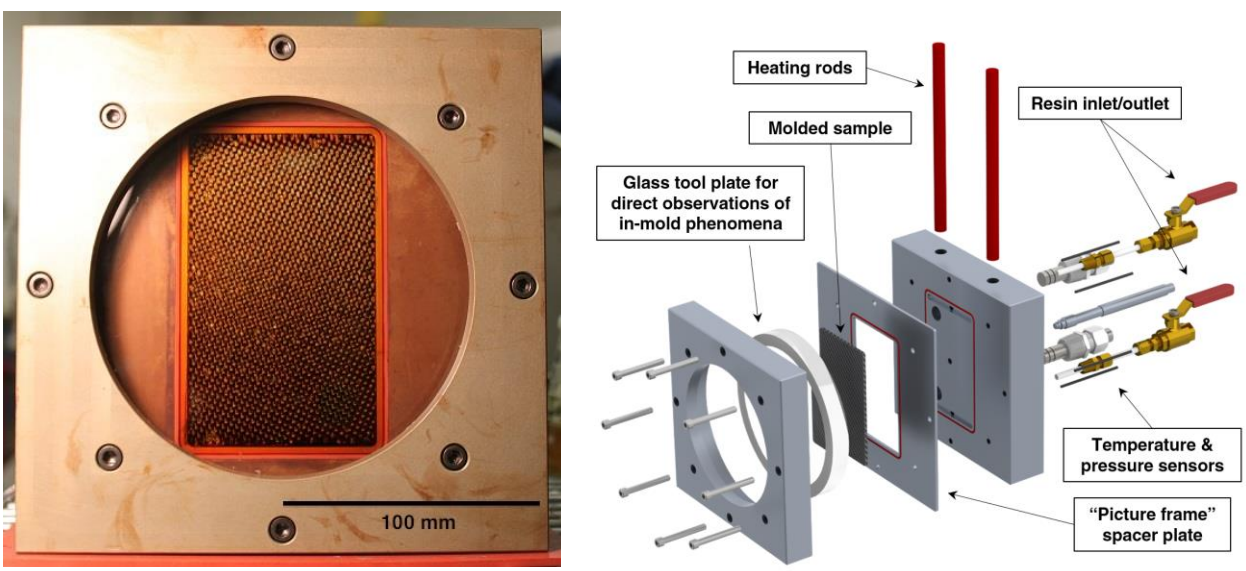

Figure 1: Front view and exploded CAD render of the lab-scale RTM.

All molded samples were reinforced with 8 layers of five-harness satin (5HS) carbon fiber fabric (364 g/m^2 areal weight, 3000 fiber/tow count, Sigmatex Ltd.) stacked in a quasi-isotropic layup.

Resin was vacuum-degassed for 45 minutes at 80°C before being loaded into a pneumatic injector (Radius 2100cc). Injections were performed at 110°C and 300 kPa, with vacuum being applied to the mold cavity both before and during injection. Excess resin was flushed through the outlet port until no bubbles remained in the mold cavity, as observed through the glass tool plate. Injection was completed by closing the outlet valve, leaving the inlet valve open, and applying a post-fill hydrostatic pressure of 450 kPa using the regulator on the injector's compressed air supply. Finally, a USB microscope was aimed at the window and used to record time-lapse videos, allowing the exact timing of porosity formation to be determined.

After de-molding, surface porosity was quantified by a measure of percent defective area. High-resolution photographs were converted to binary maps of void distribution using an open-source image processing software (ImageJ v1.48). Due to the configuration of the molding tool (with heating elements on only one side of the sample), the window-side was always cooler than the tool-side, and consequently, surface porosity appeared exclusively on the window-side of molded samples. Thus, only the window-side was considered when evaluating the surface quality. Additionally, to directly measure the magnitude of the through-thickness temperature gradient, thermocouple wires were embedded into each side of the samples cured under cycles A, E, and H, by running the wires in through the resin outlet port and placing the tips between the preform and the tool faces prior to sealing the mold.

3. CURE KINETICS MODEL

The heat of the exothermic cure reaction was measured by DSC. The degree of cure (α), which ranges from 0 for resin in the uncured state to 1 for fully cured resin, was computed using a normalized running integral of the heat release. $H(t)$ represents the heat flow over time, and the average measured total heat H_T = 473±4 J/g.

$$\alpha(t) = \frac{1}{H_T}\int_0^t H(t)dt \tag{1}$$

$$\frac{d\alpha}{dt}(t) = \frac{H(t)}{H_T} \tag{2}$$

Cure kinetics of thermoset resins are generally modeled using a rate equation that contains an Arrhenius temperature dependence times a function *f(α)*, which describes the behavior of the particular type of reaction under consideration [7].

$$\frac{d\alpha}{dt} = A\exp\left[\frac{-E_a}{RT(t)}\right]f(\alpha) \tag{3}$$

$$f(\alpha) = (1-\alpha)^n \tag{4a}$$
$$f(\alpha) = \alpha^m(1-\alpha)^n \tag{4b}$$
$$f(\alpha) = ???$$

Common choices for *f(α)* include n^{th}-order (Eq. (4a)) and autocatalytic (Eq. (4b)) expressions, but many variations have been used to capture more complex phenomena, for example the inclusion of a diffusion factor to account for the reduced reaction rate when in the diffusion-limited regime. However, for resins that undergo multiple reactions, a single-term expression as shown in Eq. (3) may not suffice to fully describe the cure kinetics behavior.

The blended resin in this study exhibits a complex set of overlapping and interdependent reactions, whose exothermic profile cannot be adequately described using Eq. (3). Modeling the cure kinetics of a variant of this resin has been previously attempted using a multi-term approach [6], but the model was unable to accurately capture dynamic behavior at varying ramp rates.

To circumvent the difficulties encountered when applying the traditional kinetics modeling approach to a complex resin, an alternative method was employed, which is purely phenomenological and does not require any specific knowledge of the chemistry. As first described by Friedman in 1964 [8], this "model-free isoconversional method" assumes only that, at every degree of cure, the reaction rate obeys some Arrhenius-type temperature dependence. As long as this

one requirement holds true, the method should theoretically be applicable to resins with any form of α-dependency (which can be unknown).

Starting from Eq. (3), assume that E_a and A are no longer constant. Let them be functions of α, and re-write the expression using a modified pre-exponential factor A' that is the product of $A(\alpha)$ and $f(\alpha)$.

$$\frac{d\alpha}{dt} = A(\alpha) exp\left[\frac{-E_a(\alpha)}{RT(t)}\right] f(\alpha) \tag{5}$$

$$\frac{d\alpha}{dt} = A'(\alpha) \exp\left[\frac{-E_a(\alpha)}{RT(t)}\right] \tag{6a}$$

$$A'(\alpha) = A(\alpha) f(\alpha) \tag{6b}$$

Taking the natural logarithm of Eq. (6a) gives Eq. (7). If we consider $1/T$ to be an independent variable x, and $ln(d\alpha/dt)$ to be a dependent variable y, then Eq. (7) is of the linear "slope-intercept" form.

$$\ln\left(\frac{d\alpha}{dt}\right) = \ln(A'(\alpha)) - \frac{E_a(\alpha)}{RT(t)} \qquad \leftrightarrow \qquad "y = mx + b"\ form \tag{7}$$

$$slope = \frac{-E_a(\alpha)}{R}$$

$$y - intercept = \ln(A'(\alpha))$$

The task of modeling the cure kinetics now consists of finding the apparent Arrhenius parameters – modified pre-exponential factor $A'(\alpha)$ and activation energy $E_a(\alpha)$ – for every value of α. For the resin in this study, first the degree of cure and cure rate were computed by Eq. (1) and (2) from DSC scans, using linear temperature ramps at 5, 7, and 10°C/minute. Figure 2 shows the results in the form of Eq. (7). For 1000 evenly spaced α values ranging from 0 to 1, the corresponding points on each DSC trace were selected and a linear fit was applied. The activation energy was extracted from

the slope of the resulting line and the modified pre-exponential factor was extracted from the y-intercept.

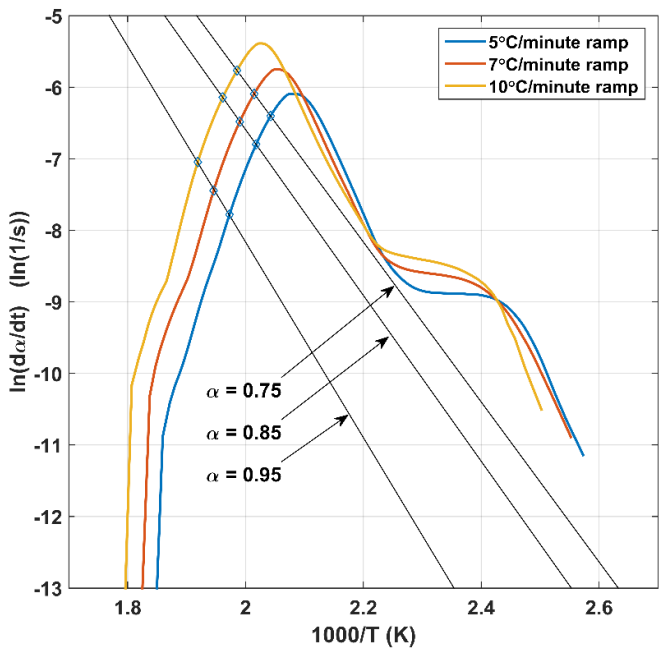

Figure 2: Isoconversional chart from dynamic DSC scans. Linear fits at some example α values are shown in black.

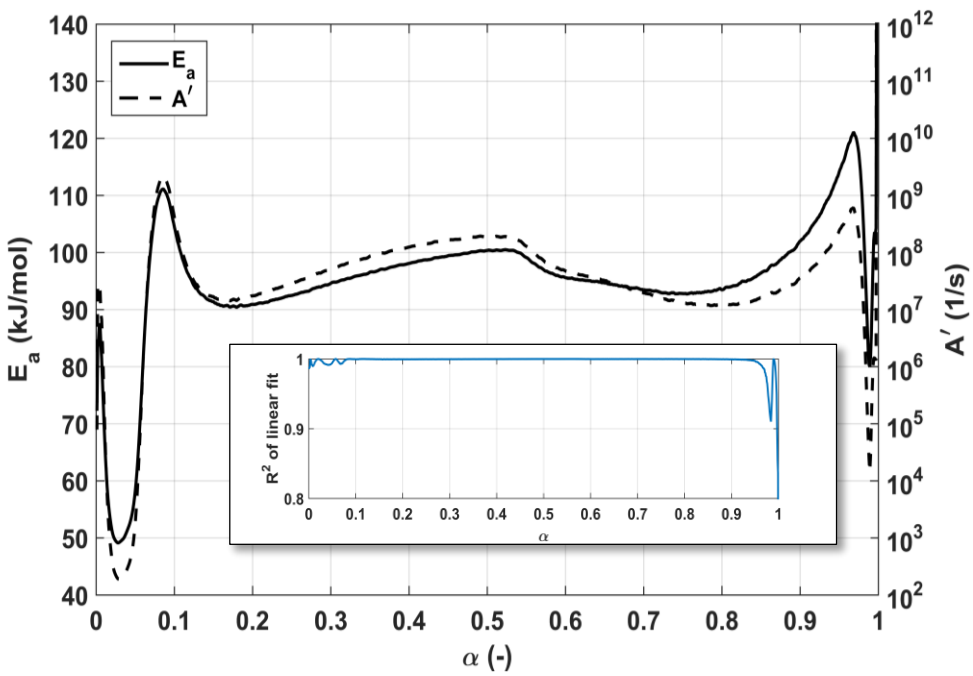

Figure 3: Experimental model parameters E_a and A' over the full range of α. Inset shows the R^2 values of the linear fits used to obtain the model parameters at each iso-α value.

Please cite this article as: M. Anders, J. Lo, T. Centea, and S.R. Nutt, **"Development of a Process Window for Minimizing Volatile-Induced Surface Porosity in the Resin Transfer Molding of a Benzoxazine/Epoxy Blend",** Journal of Advanced Materials vol. 1 (2016) ISSN 1070-9789

Figure 3 shows the resulting model parameters, as well as the R^2 values of the linear fits used to obtain the model parameters for each α. The fits were generally very close, with the exception of some error in the $\alpha > 0.95$ range. The measured end of cure is very sensitive to the particular choice of baseline used, hence the increased error in that regime, but fortunately the exact end of cure is unimportant for our purposes.

To apply the model, simply prescribe an arbitrary time/temperature cycle and use the rate equation (6a) with a numerical integration technique (e.g. forward Euler method) to stepwise compute the evolution of the degree of cure. For each time step, use the apparent Arrhenius parameters $E_a(\alpha)$ and $A'(\alpha)$ from Figure 3 corresponding to the current degree of cure. Figure 4 shows a comparison of the measured DSC data from Figure 2 and the model predictions for the same temperature cycles, indicating near-perfect agreement. Model/experiment comparisons for other temperature cycles suggest satisfactory agreement, but uncertainties arise in the measured data due to "lost heat" during temperature jumps to isothermal conditions and due to signal-to-noise issues during low-temperature isotherms or low-rate temperature ramps.

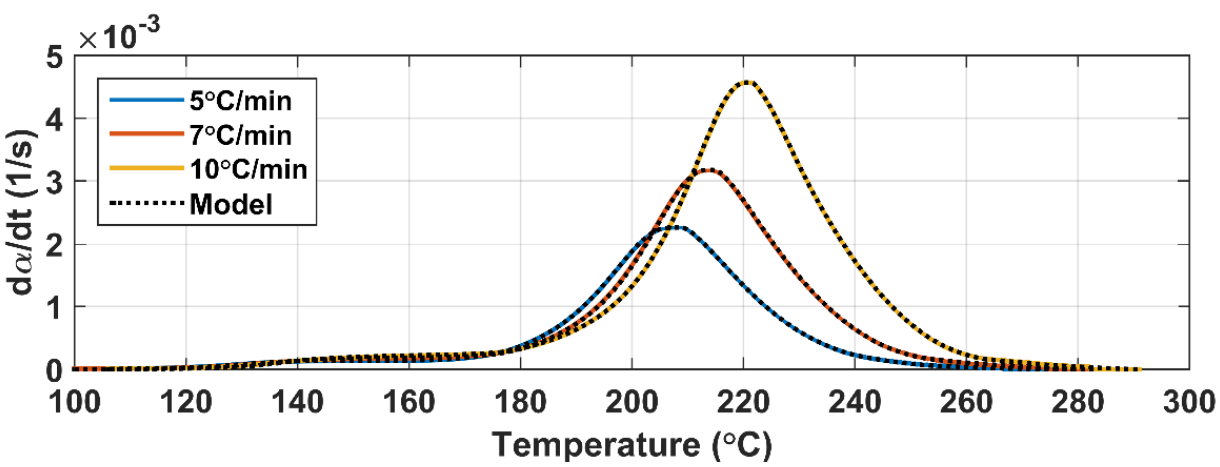

Figure 4: Comparison of measured and predicted rates of cure for the DSC scans from Figure 2.

Please cite this article as: M. Anders, J. Lo, T. Centea, and S.R. Nutt, **"Development of a Process Window for Minimizing Volatile-Induced Surface Porosity in the Resin Transfer Molding of a Benzoxazine/Epoxy Blend",** Journal of Advanced Materials vol. 1 (2016) ISSN 1070-9789

4. RESIN VOLATILE RELEASE BEHAVIOR

Figure 5 presents a comparison of data obtained by TGA, RDA, and the cure kinetics model for linear temperature ramp cure cycles at 1, 2, and 3°C/minute. The top graph shows the rate of mass loss, which initially displays a roughly exponential temperature dependence but eventually drops to zero as the resin solidifies. This mass loss is due to the evaporation of residual solvent present in the resin, and leads to void formation in closed-mold processing conditions when insufficient pressure is applied. Dots on each mass loss curve indicate the moments when evaporation had effectively stopped (defined using a threshold rate of 10^{-6} % mass per °C), and black vertical arrows point to the corresponding times on the graphs below.

The absolute magnitude of the complex viscosity, $|\eta^*|$, is shown on the middle graph. The viscosity values corresponding to the end of mass loss are found to reside in the highest order-of-magnitude and within a narrow range, suggesting that there exists a threshold mechanical state, beyond which mass loss is no longer possible due to the dissolved molecules becoming "locked in" to the growing polymer network. The threshold value of $1.7\text{-}2.0\times10^4$ Pa·s is well above the gel-point, meaning that the complex viscosity at that state is dominated by the increasing elastic modulus. Markers on each curve indicate the initial onset of gelation, defined by the moment $|\eta^*| > 1$ Pa·s, and green arrows indicate the corresponding times on the bottom graph.

The degree of cure, as predicted by the kinetics model, shows that the two phenomena of interest both occur within narrow ranges of α. The green arrows corresponding to the onset of gelation fall almost exactly at $\alpha = 0.15$, which will be referred to as α_{gel} in subsequent discussion. Similarly, the black arrows – corresponding to the end of weight loss due to resin solidification – fall in the range $\alpha = 0.30\text{-}0.34$. In subsequent discussion, a value of 0.35 is used as a conservative estimate for the critical degree of cure (designated α_{crit}) above which volatilization is expected to be minimal.

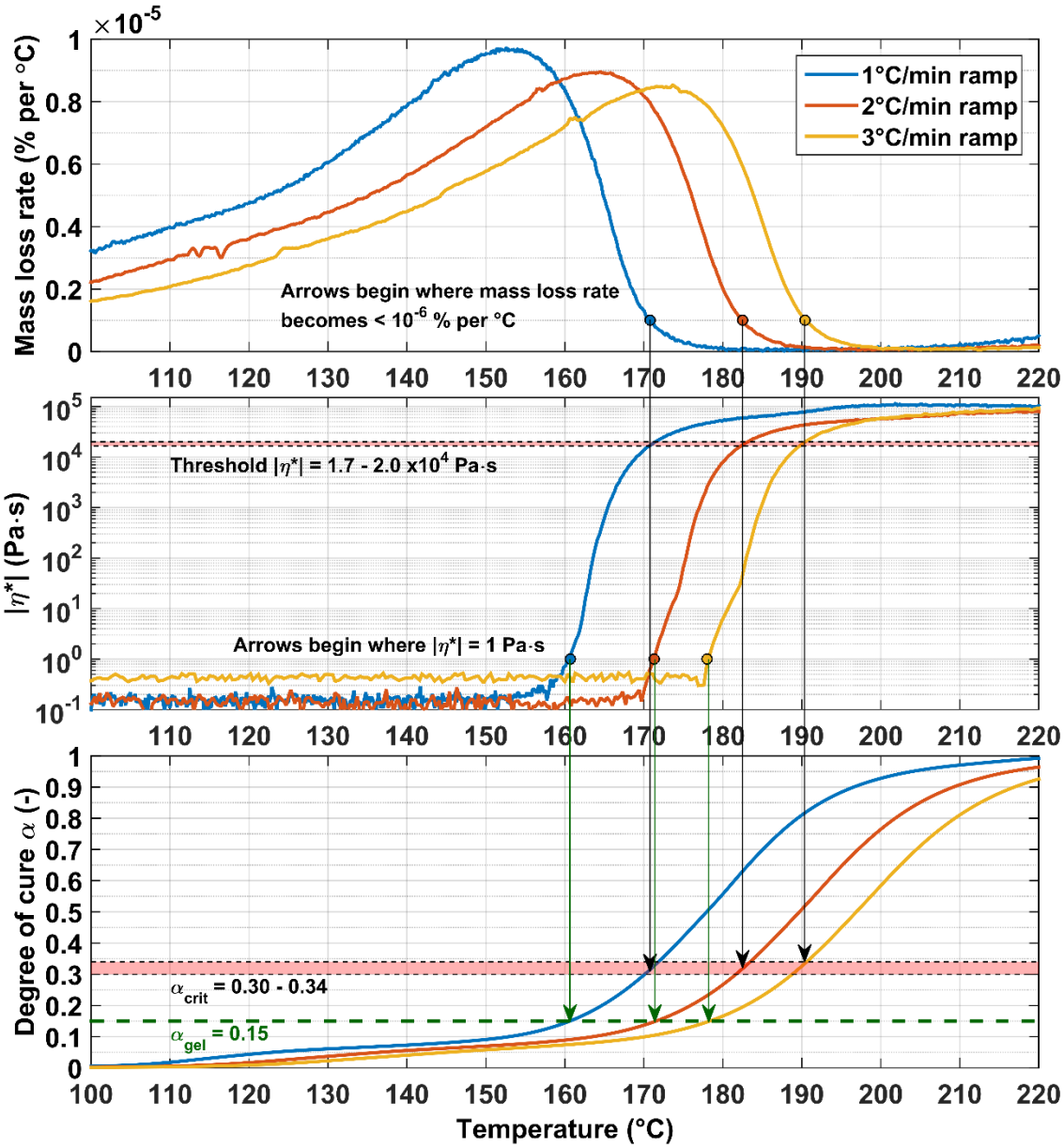

Figure 5: Mass loss rate, complex viscosity, and degree of cure, as obtained by TGA, RDA, and the cure kinetics model (respectively). Black arrows show the times when mass loss ceased, and red horizontal bands show the corresponding viscosity and degree of cure values. The onset of gelation and corresponding degree of cure are shown in green.

5. VOLATILE-INDUCED SURFACE POROSITY

By applying the criteria from the previous section to data collected from molded samples, we demonstrate the need for a two-stage cure cycle. Cycle A (Table 1) represents the baseline case,

without an intermediate temperature dwell, which results in high porosity levels. Conversely, cycle B results in minimal surface porosity.

Figure 6 shows the measured temperature and pressure data for the sample cured using the baseline cycle A, and the degree of cure (α) envelope as predicted by the kinetics model. The binary map used to determine the fractional defective surface area is shown, along with a micrograph of a representative surface void. The pressure graph shows the injector's supply pressure, the mold cavity pressure, and the "critical pressure" required to suppress volatilization. The α envelope was computed using the temperature histories of the thermocouples embedded in the part, with red indicating the hotter tool-side and blue indicating the cooler window-side.

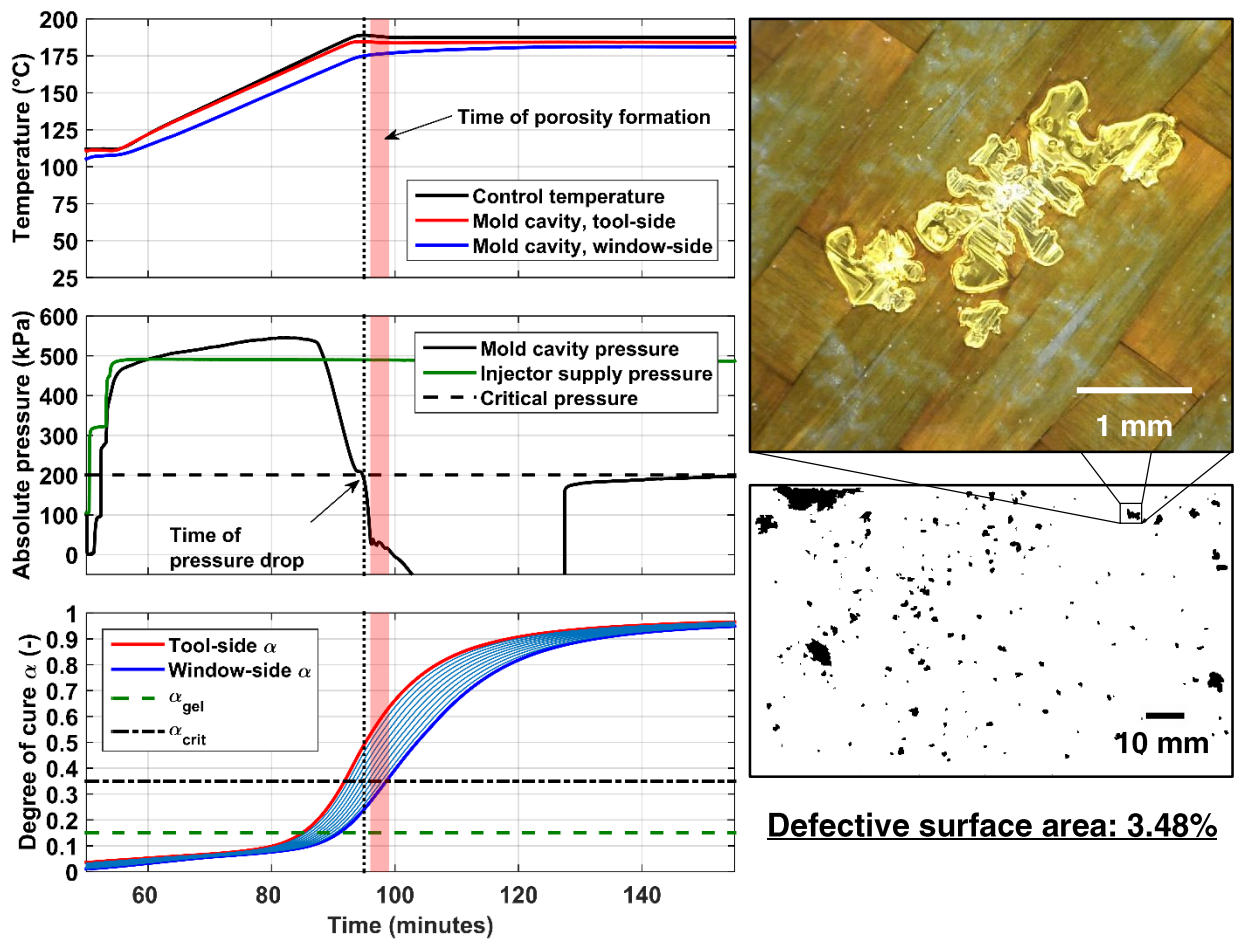

Figure 6: Temperature, pressure, and model degree of cure data for the baseline cure cycle (ramping directly to high-temperature dwell). A binary map of the surface defects is shown, along with a micrograph of a surface void.

Please cite this article as: M. Anders, J. Lo, T. Centea, and S.R. Nutt, **"Development of a Process Window for Minimizing Volatile-Induced Surface Porosity in the Resin Transfer Molding of a Benzoxazine/Epoxy Blend",** Journal of Advanced Materials vol. 1 (2016) ISSN 1070-9789

The cavity pressure, despite the application of sufficient supply pressure, dropped below the critical value at t = 95 minutes. From t = 96 – 99 minutes, surface porosity formation was observed. The degree of cure envelope shows that the pressure drop occurred when the cold-side α was below α_{crit}, thus the resin at that surface was still able to release volatiles. The formation of surface porosity ceased when the cold-side $\alpha > \alpha_{crit}$. In addition to using *in situ* observations, porosity formation can, at least qualitatively, be identified by the post-drop cavity pressure behavior. Decreasing pressure corresponds to increasing cure shrinkage, and jaggedness in the $P < P_{crit}$ regime can be attributed to void growth. Because the volatile gases are less dense than the resin, their release counteracts the density increase due to cure shrinkage. The cavity pressure in Figure 6 shows this behavior between t = 96 – 99 minutes, followed by a continued drop in pressure that eventually reaches negative values, indicating a tensile stress state in the mold cavity. The pressure jump back up to ~200 kPa at t = 128 minutes is caused by the laminate ultimately detaching from the sensor tip.

In contrast to the baseline case, cure cycle B has been demonstrated [5] to result in minimal porosity (0.12% defective area), by using an intermediate temperature dwell to slowly progress the cure reaction and reduce the amount by which the cold-side α lags when the pressure drop occurs. Cycle B, however, requires an additional 3 hours of processing time. The following section describes the procedure used to build a process map, which shows the range of intermediate dwell times and temperatures that produce behavior similar to cycle B. The characteristics of a two-stage cycle that prevent surface porosity formation are described in more detail in the context of the "optimized" cycle H in section 7.

6. PROCESS MAP

The purpose of the process map (Figure 7) is to enable the design of cure cycles that avoid surface porosity while minimizing cycle time, based on quantitative criteria for volatile release and pressure

drops. First, the baseline cycle A and the "extended dwell" cure cycles C though G are shown as dashed black lines. The times corresponding to each cycle when $\alpha = \alpha_{crit}$ are shown in blue. If cavity pressure can be maintained until the entire cure envelope has surpassed α_{crit}, minimal surface porosity can be expected. To find the maximum time that each intermediate temperature can be held, the time of pressure drop was measured experimentally for samples cured under each of the "extended dwell" cycles (C – G), given by the red line on Figure 7.

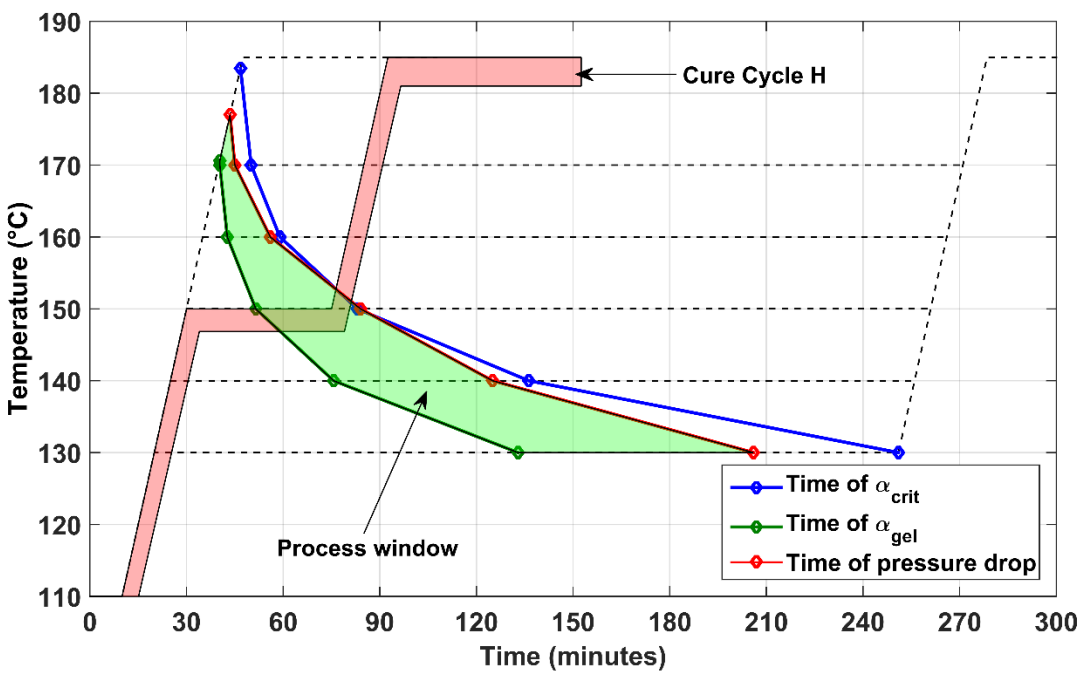

Figure 7: Process map showing times of critical degree of cure, pressure drop, and gelation, for a range of intermediate dwell temperatures. The shaded green area is the process window for intermediate dwells resulting in minimal surface porosity, and the shaded red area shows an approximate temperature envelope for Cycle H.

The location of these points – to the left of the corresponding α_{crit} points – presents an apparent discrepancy. For all intermediate dwell temperatures, the pressure drop occurred before the critical degree of cure was reached. Accordingly, the samples for cycles C – G all exhibited 2-5% surface porosity. However, for cycle B, which started the final temperature ramp 8 minutes before the pressure drop would have occurred at 130°C (as in cycle C), the pressure drop did not occur until 27

minutes into the ramp toward 185°C, and the surface only developed porosity over 0.12% of the area.

The explanation for this delayed pressure drop lies in the thermal expansion of the resin during temperature ramps. In the case of Figure 6 (cycle A), the cavity pressure increased during the temperature ramp, but only slightly. Because the resin is initially liquid and connected to a constant-pressure supply, as it undergoes thermal expansion in the mold cavity, the resin has the ability to back-flow through the inlet port to maintain equilibrium hydrostatic pressure. However, once the resin has gelled, it loses the ability to flow. In the case of cycle B, the resin gelled during the intermediate dwell at 130°C and the cavity pressure began to decrease below the supply pressure due to cure shrinkage. However, when the temperature was ramped upwards, thermal expansion temporarily caused the cavity pressure to increase, delaying the pressure drop long enough for the cold-side α to surpass α_{crit}.

The phenomenon of thermal expansion is critical to maintaining mold pressure, because after the resin has gelled, the supply pressure loses all ability to influence cavity pressure (as clearly evidenced by the pressure drops that occur in every test). To exploit the effect of thermal expansion on cavity pressure, we must first gel the resin at an intermediate temperature, and only then ramp to the final cure temperature. We can therefore define the minimum times for intermediate dwells by α_{gel}, which is indicated by the green points on Figure 7.

The green shaded region – between the gel times and the pressure drop times – represents the allowable "process window" for intermediate temperature dwells. For any of the temperatures in the range shown, a dwell shorter than the gel time will be ineffective (resulting in behavior similar to that of cycle A), and a dwell that's too long will also result in a pressure drop before $\alpha > \alpha_{crit}$. Dwell

times between the two limits, however, will have delayed pressure drops, which gives the resin additional time to reach or exceed α_{crit}.

7. CURE CYCLE DESIGN

To use the process map for cure cycle design, consider the temperature envelope bounded by the hottest and coldest regions in the mold cavity. The intermediate dwell must be held at least until the cold side reaches α_{gel}, but the hotter side must be used to conservatively predict the maximum dwell time, since pressure drops are determined by the cumulative contribution of cure shrinkage through the entire laminate. Because the process window gets narrower at higher temperatures, RTM tools with wider temperature envelopes will require longer, lower-temperature holds to meet this requirement. The red shaded region on Figure 7 shows the "optimized" cure cycle H (from Table 1), which uses a 45 minute dwell at 150°C. The width of the temperature envelope is approximated using a cold-side temperature lag of 3% (relative to room temperature) and a time lag of 4 minutes. The 45 minute dwell ends before the pressure drop would occur, and the cold side is well past α_{gel}. Figure 8 shows the results of the RTM sample fabricated using cycle H.

At the time of the pressure drop, the entire degree of cure envelope for cycle H was above α_{crit}, and consequently, the sample exhibited 95% less surface porosity than the case of cycle A (Figure 6). The few surface voids that did appear in cycle H were in the form of barely visible, shallow dimples, as opposed to the large sub-surface bubbles that formed under cycle A.

The beneficial effect of the post-gelation temperature ramp can be understood by considering the following simple approximation for relative density [9].

$$\frac{\rho}{\rho_0}(\alpha, T) = 1 + c_1(T - T_0) + c_2(\alpha - \alpha_0) \tag{8}$$

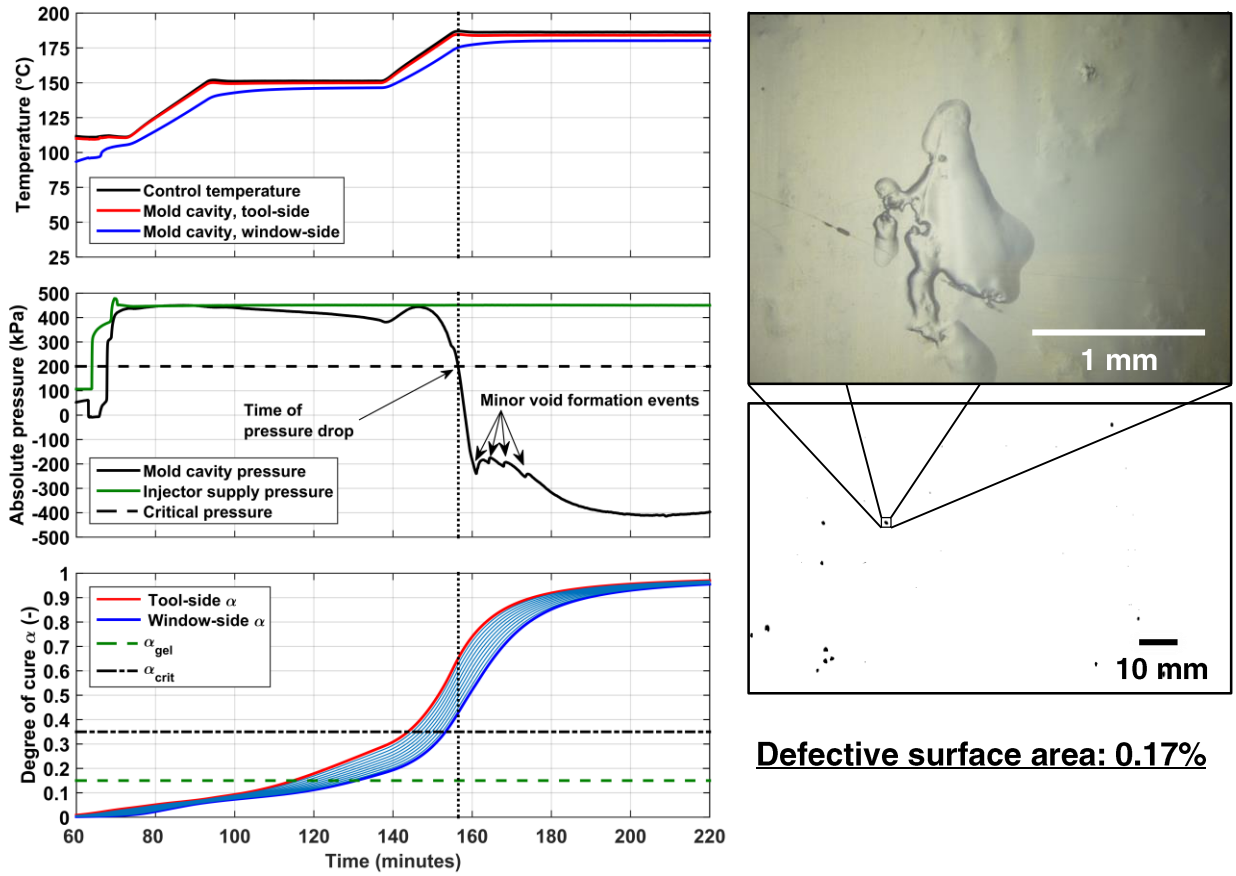

Figure 8: Temperature, pressure, and model α for cure cycle H (45 minutes intermediate dwell at 150°C).

Eq. (8) assumes linear changes in relative density due to thermal expansion and cure shrinkage (which is assumed to progress linearly with α). Using T_0 = 25°C and α_0 = 0 for the reference state ρ_0, a total shrinkage value of 1% (from [6]), and a thermal expansion coefficient for a similar resin from [10], Figure 9 was generated for the cure cycles A, E, and H.

Because resin can no longer flow after the gel point, it is the density increase beyond that point which causes the pressure drop. The resin gels at ~170°C for cycle A, and the pressure drop occurs soon after, when the cold-side α is still < α_{crit}. For an extended dwell at 150°C, gelation occurs during the dwell, and then continued cure shrinkage causes a pressure drop. For cycle H, however, gelation is induced at 150°C, but then the temperature ramp causes the cure envelope to move parallel to the iso-ρ contours. This acts to increase α without increasing density, pushing the entire α envelope

above α_{crit} before the pressure drop occurs. The "hump" in cavity pressure during the final temperature ramp in Figure 8 can be directly attributed to the temporarily decreasing density seen during the corresponding ramp in Figure 9.

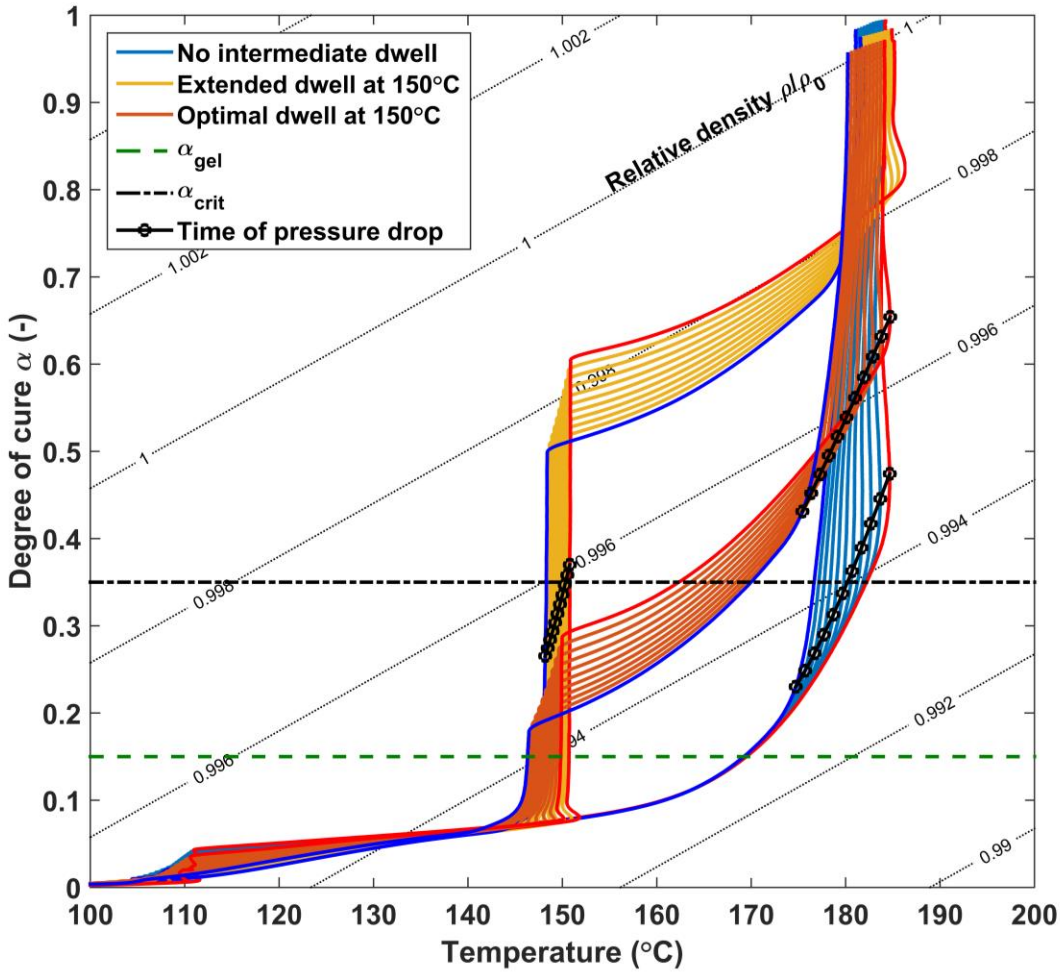

Figure 9: Degree of cure vs. temperature envelopes for cure cycles with 0, 45, and 120 minute intermediate dwells at 150°C before the high-temperature dwell. Diagonal contour lines indicate relative density, which varies with both temperature and degree of cure as described by Eq. (8).

8. CONCLUSIONS

The value of the process map is to enable improvements in cure cycle design by describing the phenomena relevant to surface porosity formation over a wide range of temperatures. A cure cycle was designed that reduced the required intermediate dwell time by a factor of four (45 min. for cycle

H vs. 180 min. for cycle B), and was demonstrated to be almost as effective at preventing surface porosity (0.17% for cycle H vs. 0.12% for cycle B).

By considering the entire temperature envelope, use of the process map can take into account the limitations of any particular RTM tool's heating scheme. For larger temperature gradients, simply dwell at lower temperatures for longer times, to ensure that the entire part falls within the required process window.

There are, however, some limitations to the approach described here. First, only a through-thickness temperature gradient is considered. This one-dimensional simplification ignores in-plane gradients, and thus complex part geometries and temperature distributions may require a more sophisticated description. Furthermore, the time of pressure drop has only been experimentally determined for the particular molding tool used in this study. Since the timing of this event may vary between tools (due to geometry, rigidity, part thickness, mold pressure, etc.), a more comprehensive description of density changes and related pressure behavior is desired. Finally, we do not consider varying ramp rates, which could also influence the pressure behavior. The 2°C/min ramp used coincidentally causes thermal expansion to occur at roughly the same rate as cure shrinkage (see the slope of the "optimal dwell" envelope in Figure 9 compared to the iso-ρ contours), but the ramp rate could certainly be changed to influence the timing of the pressure drop.

Overall, the methods used in this study have potential relevance to a wide range of composite molding applications. First, the "model-free" kinetics characterization technique is advantageous because it does not require any knowledge of the reaction mechanism. It can, in theory, be used for any resin that obeys an Arrhenius temperature dependence, including complex formulations that may undergo multiple overlapping reactions. Second, the use of an RTM with a transparent tool-plate can provide insight into in-mold phenomena, which are generally not observable *in situ* due to

the "black box" nature of standard metal RTM tools. Finally, by combining a cure kinetics model with defect-formation criteria developed through thermal characterization (TGA, RDA) and from *in situ* observations, porosity formation can be predicted and guidelines can be developed for cure cycle modifications that reduce defect levels.

Acknowledgements: The authors acknowledge financial and material support from the M.C. Gill Composites Center. Undergraduate research assistant Matthew Thomas contributed to the experimental characterization of the resin.

References:

[1] Kruckenberg T, Paton R. Resin Transfer Moulding for Aerospace Structures. Springer Netherlands; 1998. doi:10.1007/978-94-011-4437-7.

[2] Ruiz E, Achim V, Soukane S, Trochu F, Bréard J. Optimization of injection flow rate to minimize micro/macro-voids formation in resin transfer molded composites. Compos Sci Technol 2006;66:475–86. doi:10.1016/j.compscitech.2005.06.013.

[3] Pearce N, Guild F, Summerscales J. A study of the effects of convergent flow fronts on the properties of fibre reinforced composites produced by RTM. Compos Part A Appl Sci Manuf 1998;29:141–52. doi:10.1016/S1359-835X(97)00041-9.

[4] Ishida H, Allen DJ. Mechanical characterization of copolymers based on benzoxazine and epoxy. Polymer (Guildf) 1996;37:4487–95. doi:10.1016/0032-3861(96)00303-5.

[5] Anders M, Lo J, Centea T, Nutt S. VOLATILE-INDUCED VOIDS IN RTM PROCESSING FOR AEROSPACE. 12th Int. Conf. Flow Process. Compos. Mater., Enschede, NL: 2014.

[6] Centea T, Lo J, Anders M, Nutt SR. Process Modeling for Resin Transfer Molding of a Modified Heterocyclic Phenolic/Epoxy Blended Resin. ASC 2014 Proc., 2014.

[7] A. Yousefi, P. G. Lafleur RG. Kinetic Studies of Thermoset Cure Reactions : A Review. Polym Compos 1997;18.

[8] Friedman HL. Kinetics of thermal degradation of char-forming plastics from thermogravimetry. Application to a phenolic plastic. J Polym Sci Part C Polym Symp 1964;6:183–95. doi:10.1002/polc.5070060121.

[9] Brauner C, Soprano P, Herrmann a. S, Meiners D. Cure-dependent thermo-chemical modelling and analysis of the manufacturing process of an aircraft composite frame. J Compos Mater 2014. doi:10.1177/0021998314527777.

[10] Yang L, Zhang C, Pilla S, Gong S. Polybenzoxazine-core shell rubber-carbon nanotube nanocomposites. Compos Part A Appl Sci Manuf 2008;39:1653–9. doi:10.1016/j.compositesa.2008.07.004.